NRL Report 6899

The Infrared Radiation from Solid-Propellant Rocket Motors

G. L. HARVEY AND J. D. BURCH

Infrared Branch
Solid State Division

May 29, 1969

APPROVED FOR PUBLIC RELEASE - DISTRIBUTION UNLIMITED

NAVAL RESEARCH LABORATORY
Washington, D.C.

CONTENTS

Abstract	ii
Problem Status	ii
Authorization	ii
INTRODUCTION	1
TEST SITE	1
DESCRIPTION OF EQUIPMENT	2
Radiometers	2
Rapid-Scanning Spectrometer	13
SPECTROMETER SYSTEM CALIBRATION AND RESOLUTION	15
SCANNING SPECTROMETER DATA REDUCTION	19
ACCURACY	19
Radiometer	19
Rapid-Scanning Spectrometer	20
DISCUSSION OF RESULTS	21
Radiometric Data	21
Spectral Data	23
CONCLUSIONS	31
ACKNOWLEDGMENTS	32
REFERENCES	32
APPENDIX A — Considerations in the Reduction of Radiometric Data	33

ABSTRACT

The infrared radiation in the spectral region of 1.45 to 20 μm from stationary solid-propellant rocket motors of the Sidewinder type was measured using two radiometers and a rapid-scanning spectrometer. The measurements were made at a range of 200 m at aspect angles of approximately 90°, 45°, and 0° to the flame. The emission spectra were found to be similar to those of other kinds of hydrocarbon flames.

PROBLEM STATUS

This is one of two reports on the radiation from rocket motors. A future NRL report will give the results of measurements on liquid-propellant motors. This work is part of a continuing program on infrared countermeasures.

AUTHORIZATION

NRL Problem R06-38
Project SF 23-372-006-9292

Manuscript submitted February 19, 1969.

THE INFRARED RADIATION FROM SOLID-PROPELLANT ROCKET MOTORS
[Unclassified Title]

INTRODUCTION

Guided antiship missiles are an important threat to the Navy. To classify, detect, and track these missiles by infrared methods it is important to know the spectral distribution, the radiant intensity, and the time characteristics of the infrared radiation from the missile plume radiation.

This report describes the results of tests made to determine the spectral radiant intensity of solid-propellant motors, such as those used on the Sidewinder missile. The seven solid-propellant motor tests were part of a larger program, which was concerned primarily with liquid fuel propellants.

In addition to the data taken by NRL and reported here, data were taken by the following organizations:

- Naval Research Laboratory Acoustics Division — sound intensity at various angles;
- Naval Research Laboratory, Applications Research Division — area of infrared and visible plume;
- Block Engineering, Inc. — spectral radiation measurements;
- Naval Ordnance Station, Code DCL — firing of motors and monitoring of motor parameters;
- Scope, Inc. — intensity variations in PbS band.

These tests were performed under static conditions, and the applicability of the data for moving rockets needs to be verified.

TEST SITE

The tests were conducted at the Naval Ordnance Station at Indian Head, Maryland. Figure 1 is a map of the test site showing the location of the test stand at point A; site 1, 198 m inland from the stand; sites 2 and 3 across the Mattawoman Creek at ranges of 500 and 1105 m, respectively; and site 4 on a dock at Stump Neck 3638 m downstream. Only site 1 was used by NRL during the solid-propellant tests.

The measurements were made at a range of 198 m and at aspect angles of 90°, 45°, and 0° relative to the head-on aspect of the motor. The solid-propellant motors were secured to the stand shown in Fig. 2. The stand was 20 ft above the ground level and had a rotatable table on top for setting the horizontal aspect angle. The missile body shown in this figure was removed for the tests.

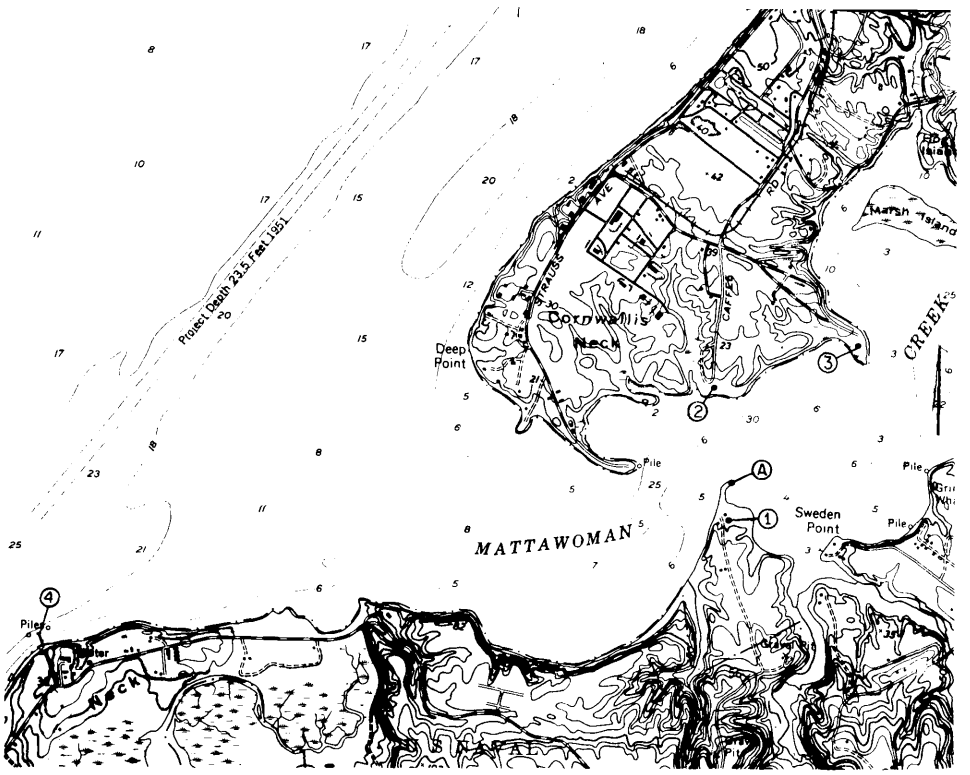

Fig. 1 - Map of test site at Naval Ordnance Station, Indian Head

DESCRIPTION OF EQUIPMENT

Radiometers

One of the radiometers (designated as instrument A in this report), shown in Fig. 3, was assembled by NRL personnel. It consisted of an optical system using an 8-in.-diameter, $f/1.9$ collector with a thermistor detector. The chopping frequency was 80 Hz. The theoretical field of view was 6.9 x 6.9 milliradians (mrad), while the effective field of view, measured by the method described in Appendix A, was 11.1 x 11.1 mrad. The electronics consisted essentially of a Brower Model 131 lock-in amplifier. The output signal was recorded on a Heath recorder. Interference filters were inserted in the beam between the chopper and the detector. The spectral transmissions of these filters are shown in Figs. 4 through 8. The other radiometer was a Barnes Model R-8T2 dual-channel instrument (designated as instrument B in this report), shown in Fig. 9. Channel 1 had a six-position filter holder, and Channel 2 was unfiltered. The detector in Channel 1 was a hyperimmersed thermistor with a germanium lens, antireflection coated to peak at 10 μm. The detector for Channel 2 was an immersed thermistor detector with a germanium lens antireflection coated to peak at 10 μm. The spectral transmission of the filters used with Channel 1 are shown in Figs. 8 and 10 through 13. It was necessary to add a baffle plate over the front of the Barnes radiometer to attenuate the signal, so that the electronic system did not overload. The radiation was attenuated by a factor of approximately seven.

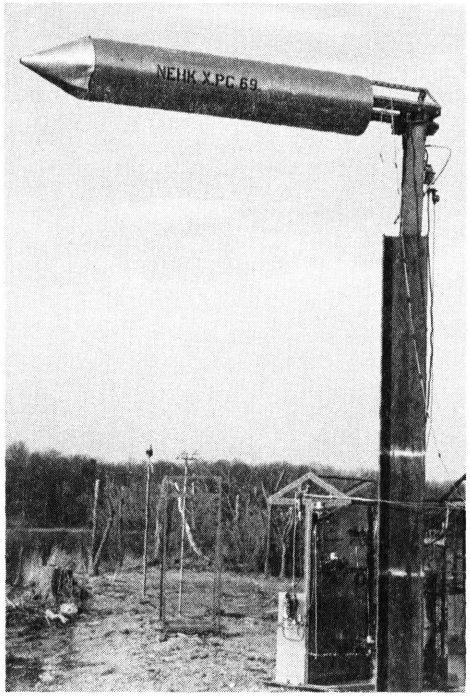

Fig. 2 - Test stand for rocket motors

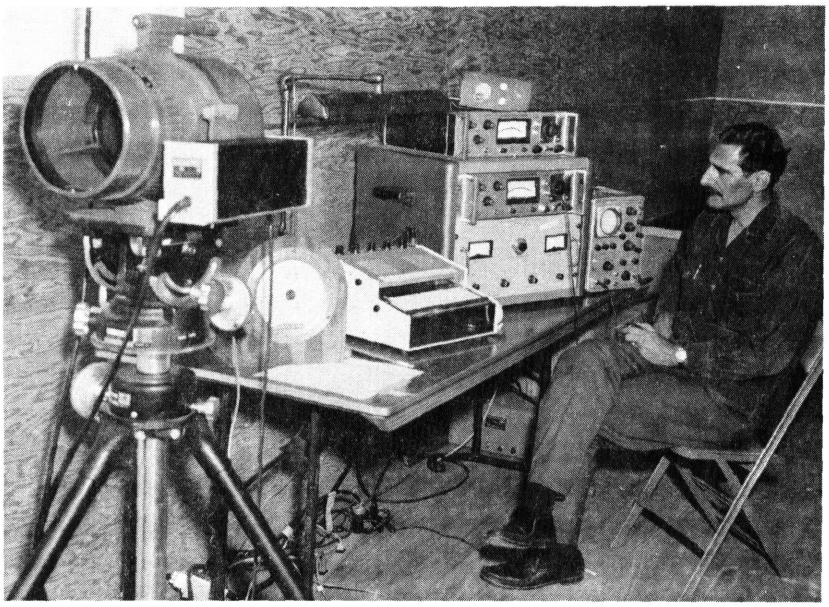

Fig. 3 - NRL radiometer A

Fig. 4 - Transmission of interference filter 2A, 7.7 to 20.5 μm

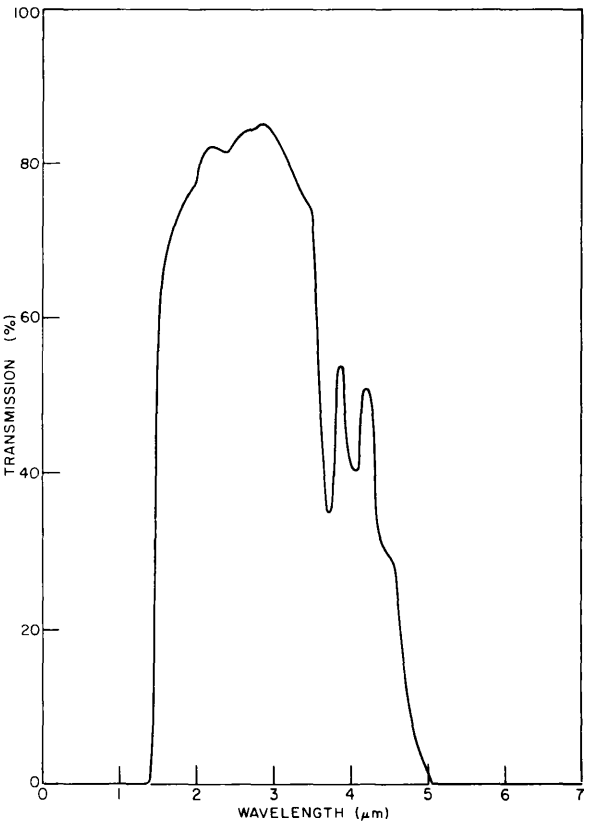

Fig. 5 - Transmission of interference filter 3A, 1.48 to 4.6 μm

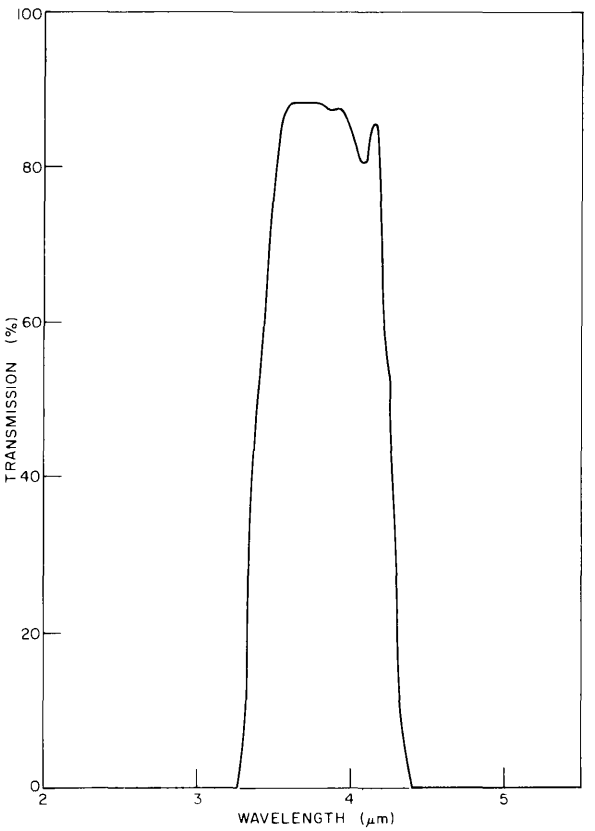

Fig. 6 - Transmission of interference filter 4A, 3.38 to 4.38 μm

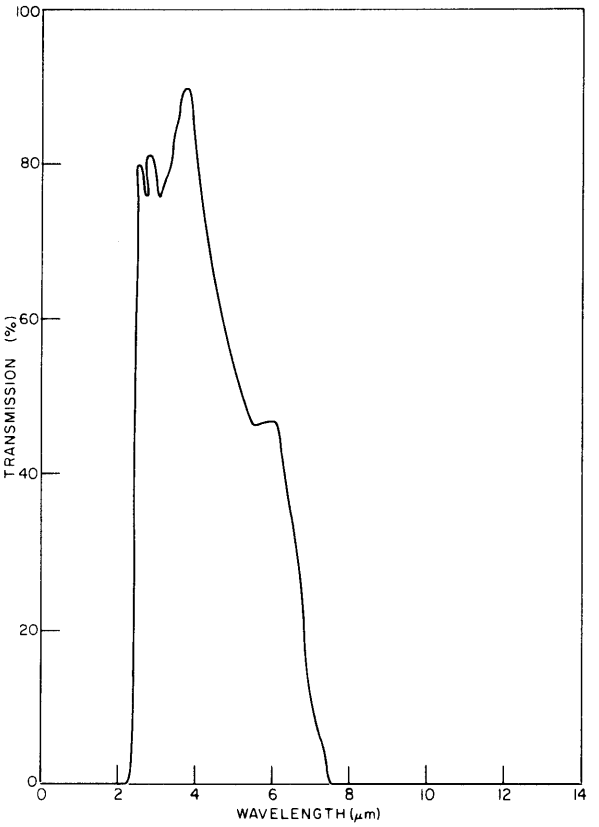

Fig. 7 - Transmission of interference filter 5A, 2.9 to 6.65 μm

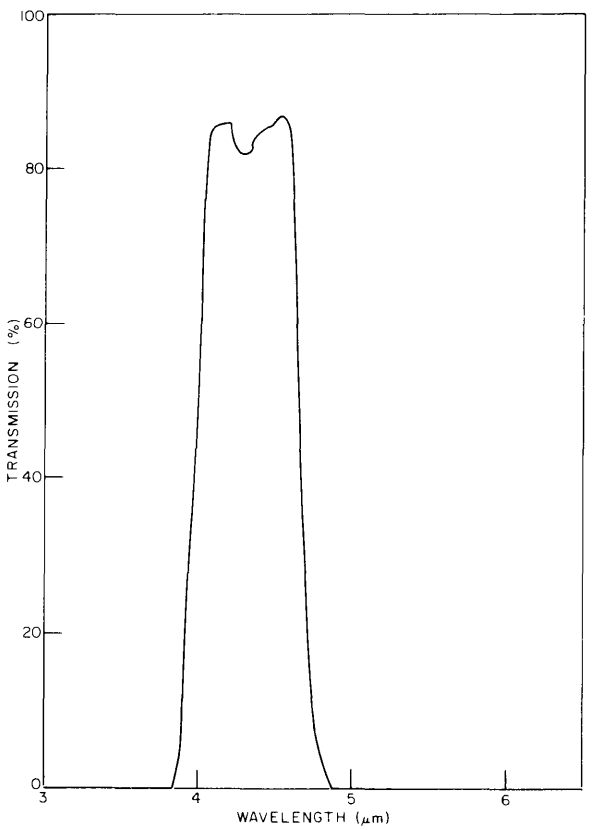

Fig. 8 - Transmission of interference filter 6A and 6B, 3.95 to 4.69 μm

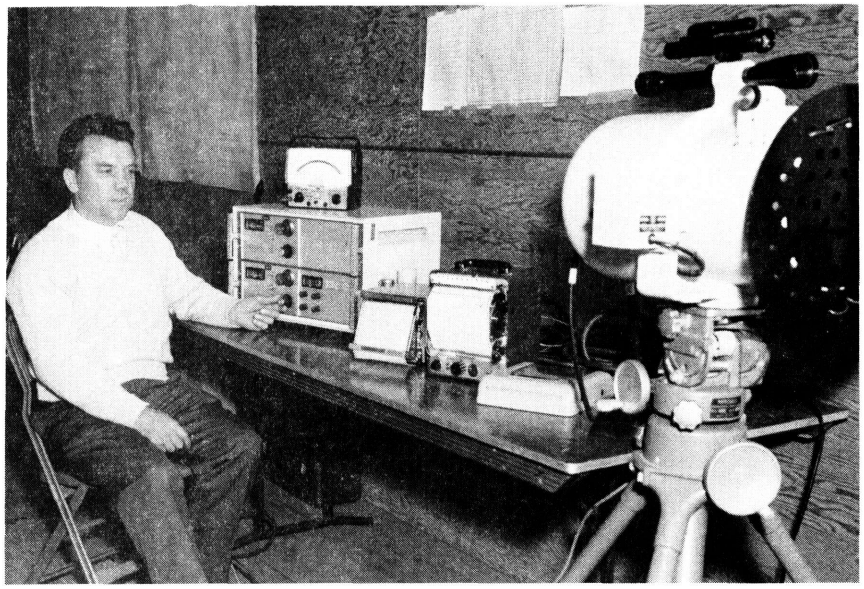

Fig. 9 - Barnes R8T-2 radiometer with attenuator

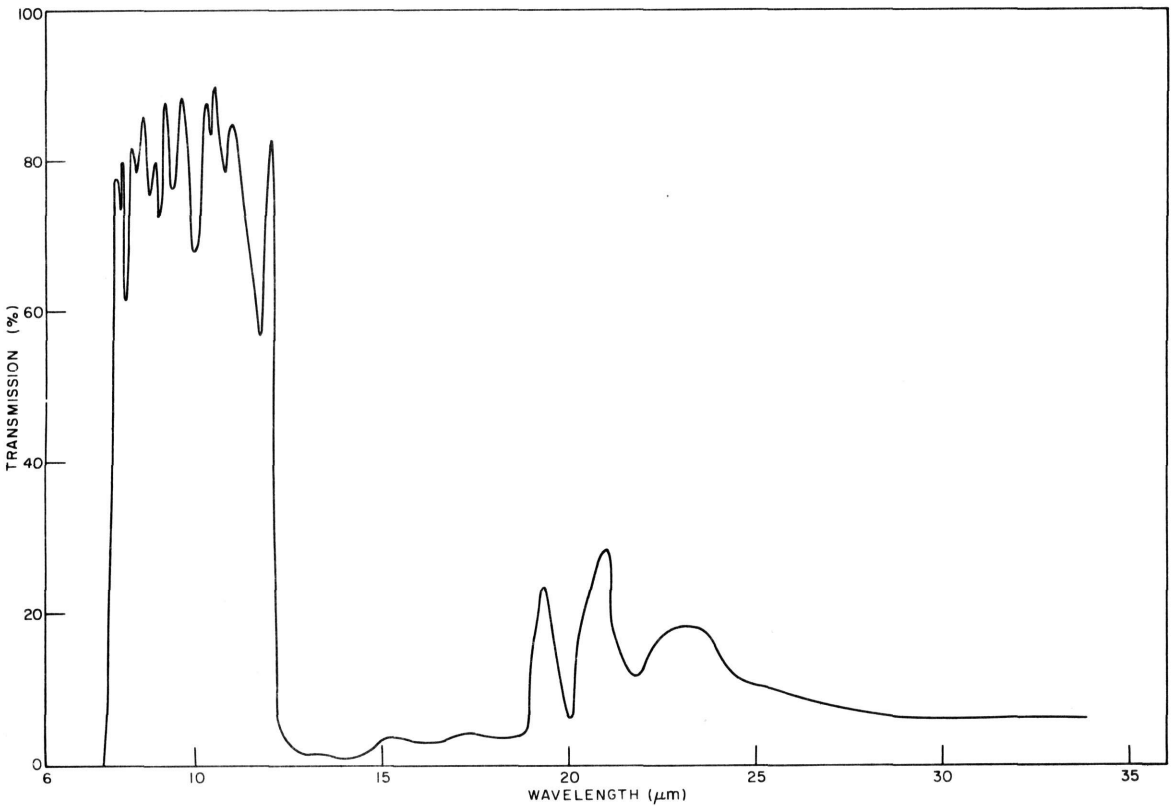

Fig. 10 - Transmission of interference filter 2B, 7.7 to 12.15 μm

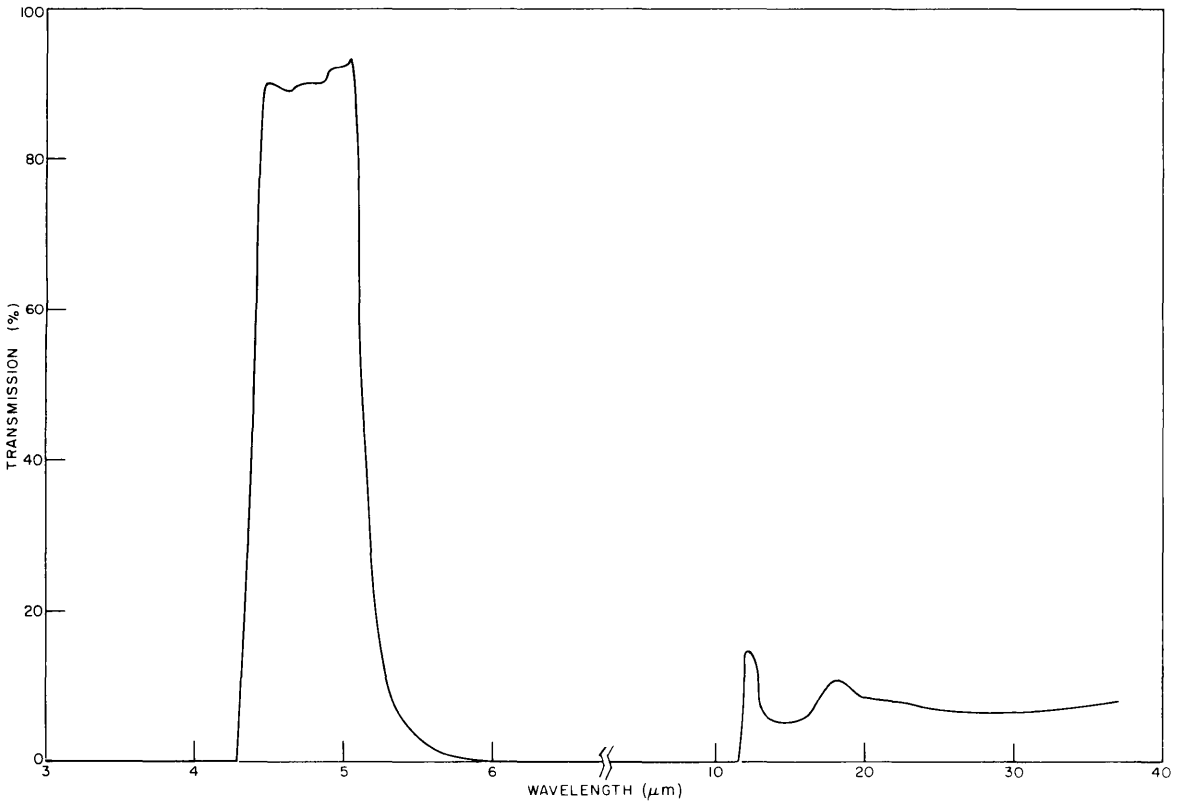

Fig. 11 - Transmission of interference filter 3B, 4.38 to 5.19 μm

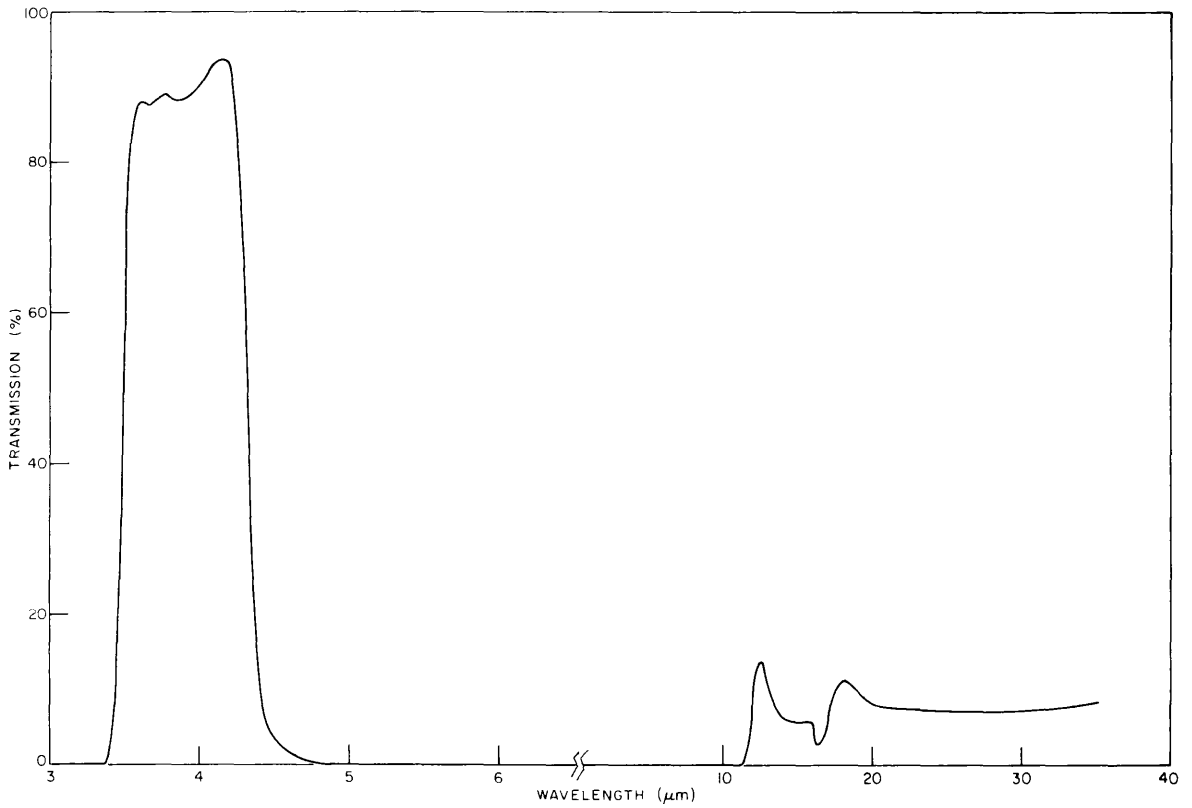

Fig. 12 - Transmission of interference filter 4B, 3.47 to 4.33 μm

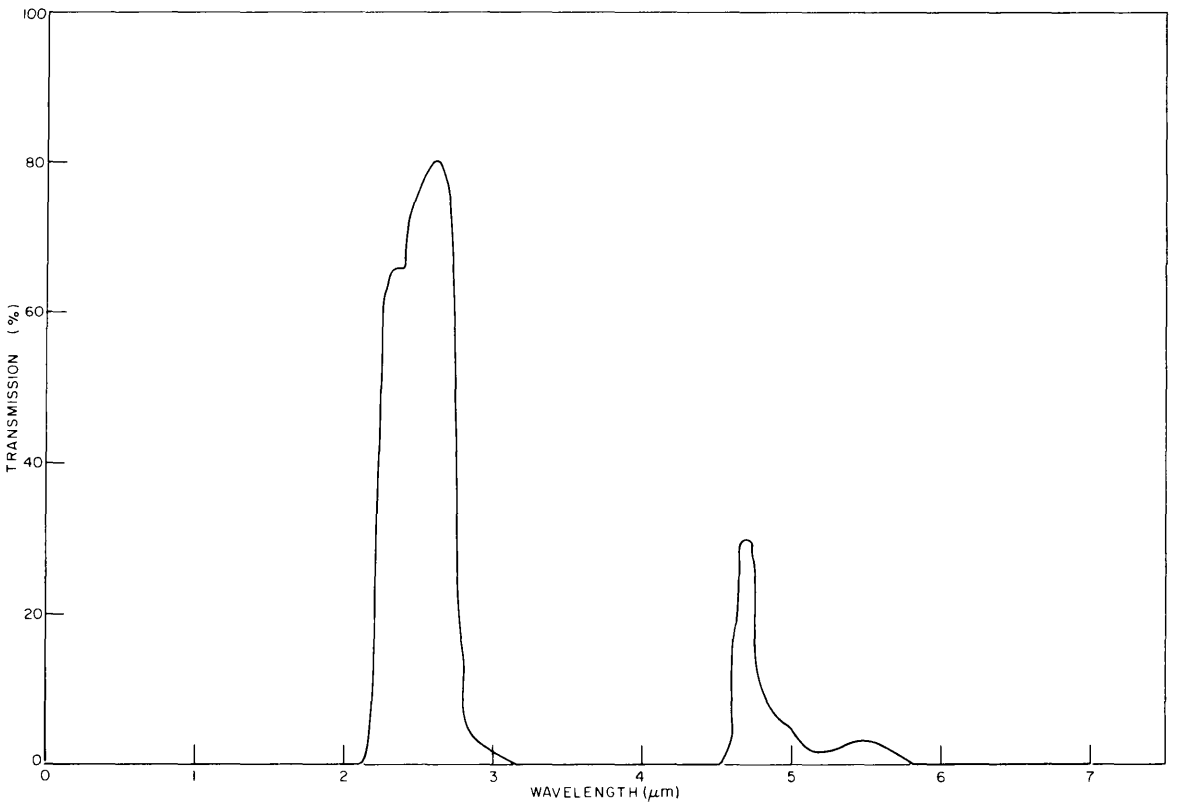

Fig. 13 - Transmission of interference filter 5B, 2.21 to 2.57 μm

Rapid-Scanning Spectrometer

The spectrometer was basically a Perkin-Elmer Model 98 single-pass monochromator, modified for rapid scanning and equipped with a cooled indium-antimonide detector. This component was on loan from the Infrared Group at the Naval Ordnance Laboratory in White Oak, Maryland. Figure 14 is a photograph of the instrument.

The collecting optics of the rapid scanning, spectrometer system (Fig. 15) consist of a 5.4-in.-diameter focusing mirror and an ellipsoidal Newtonian reflector for focusing the radiation on the entrance slit. The effective collecting area of the focusing mirror is 133 cm^2, and its focal length is 54 cm. The dimensions of the rectangular entrance slit are 1 mm wide by 5 mm high. The maximum field of view thus determined for the system is 1.9 mrad wide by 9.3 mrad high. The effective field of view was not measured and is slightly less than this figure because of optical misalignment and the inequality of the f numbers of the external and internal optics.

The modified, single-pass, spectrometer system is shown schematically in Figs. 16 and 17 (1). Radiation is chopped at 4000 Hz by the chopper C before passing through the entrance slit S_1, which was kept at a 1-mm width. The prism P is of lithium fluoride. Mirror M_2 is an oscillating Littrow mirror, cycling at a rate of 4 Hz. Its angular velocity as a function of time is shown in Fig. 18. A forward-going and backward-going scan is made during each cycle of the Littrow, and it takes about 0.1 sec for a single scan. The exit slit was set at 1 mm during all the measurements. The radiation from the exit slit is focused on the detector, as shown in Fig. 17. A liquid-nitrogen cooled, indium-antimonide detector was used, which limited the long-wavelength response of the

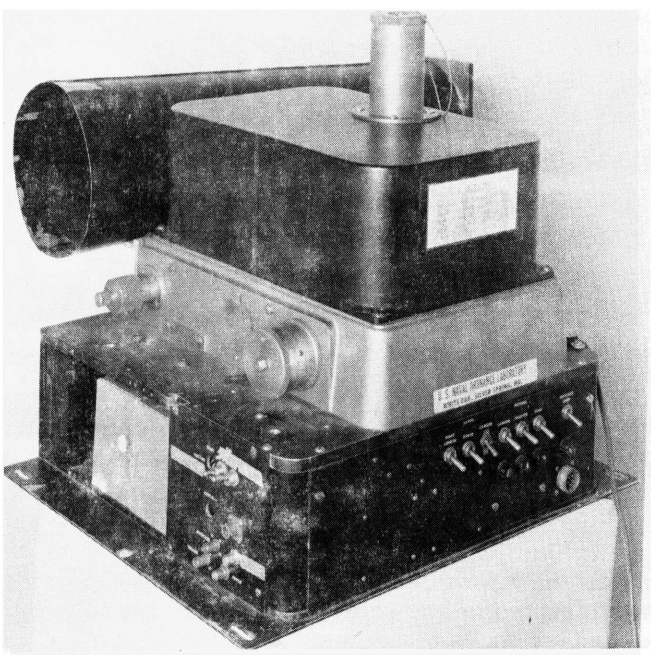

Fig. 14 - Rapid-scanning spectrometer

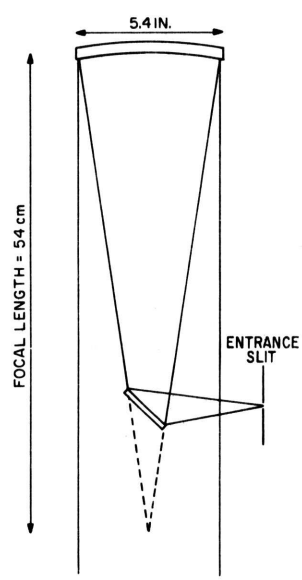

Fig. 15 - Collecting telescope of rapid-scanning spectrometer

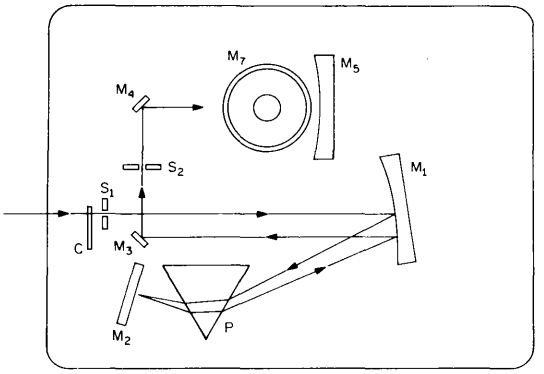

Fig. 16 - Internal optical path of spectrometer

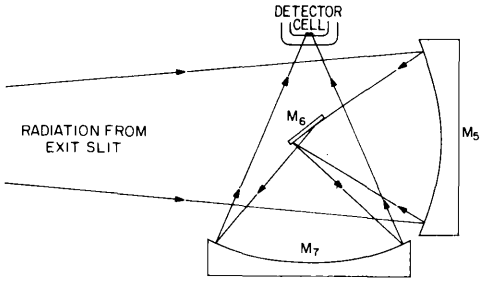

Fig. 17 - Spectrometer exit optics

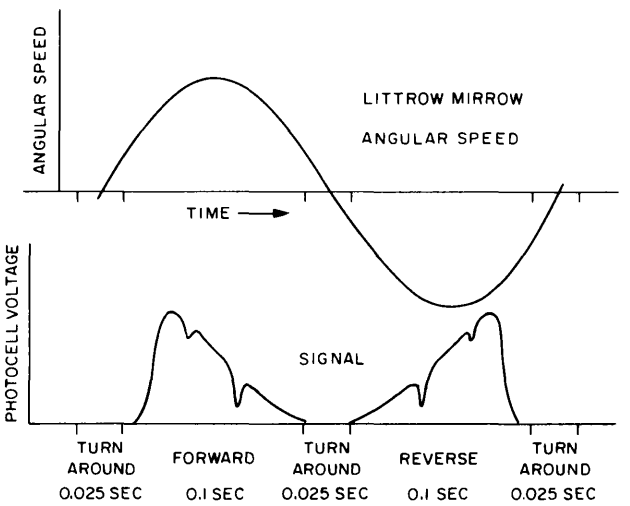

Fig. 18 - Littrow mirror scanning cycle

instrument to about 5.6 μm. The system was flushed with dry nitrogen to prevent condensation and frosting.

There are two supplementary electro-optical systems associated with the spectrometer. A photodiode-light system, combined with a reflecting mirror on the drive shaft of the Littrow mirror, provides a trigger pulse for the oscilloscope at the beginning of each forward-going spectrum. A second system, shown schematically in Fig. 19, provided the wavelength marker. The mirror M is mounted on the same shaft as the Littrow mirror, and thus its angular position corresponds to the angular position of the Littrow mirror. As the Littrow mirror scans the spectrum, light from the narrow slit S is reflected by M across the modulating reticle pattern R (Fig. 20) and is imaged on the phototube by the lens L. The light beam sweeps across R once during each scan, producing a modulation pattern of some 70 "pips." This signal from the phototube is amplified and displayed on

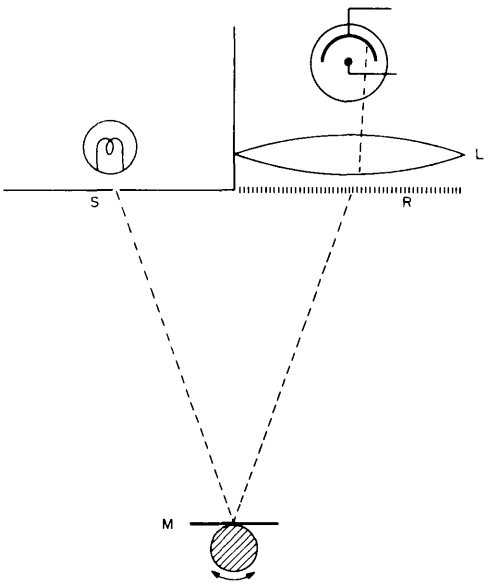

Fig. 19 - Wavelength marker system

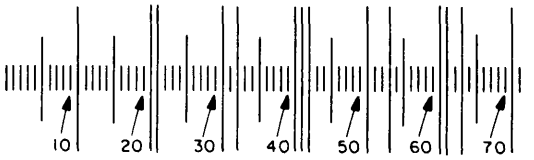

Fig. 20 - Wavelength marker reticle pattern, R

the dual-beam oscilloscope tube above the target signal. Standard-wavelength calibration procedures enable one to correlate wavelength with position along the wavelength marker.

The electronics and the recording system associated with the spectrometer consist of an amplifier and a dual-beam oscilloscope equipped with a camera. The wideband, variable-gain amplifier has a bandpass (3 dB points) from 2 Hz to 45 kHz. One scan was photographed during each missile firing.

SPECTROMETER SYSTEM CALIBRATION AND RESOLUTION

The wavelength calibration of the spectrometer was made in the field under the actual operating conditions. The wavelength corresponding to each pip marker was determined using standard gas-absorption cells (2). The results are shown in Fig. 21.

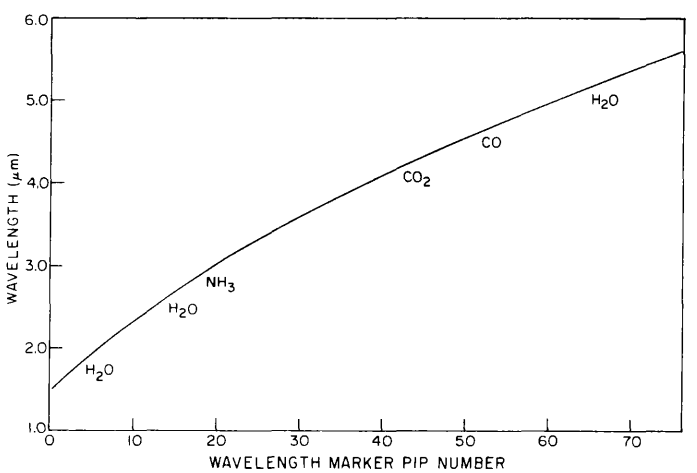

Fig. 21 - Wavelength calibration, NOL rapid-scanning spectrometer, June 8, 1968

The amplitude calibration of the instrument (spectral system calibration) was accomplished at the same time as the wavelength calibration. It was assumed to be constant throughout the data runs.

Because of the short distance to the target (200 m) and the relatively small field of view of the system (1.9 mrad x 9.3 mrad), it was decided to calibrate the instrument in terms of N_λ, the apparent spectral radiance of the target (W/cm^2 sr μm). No attempt was made to "correct" the data for atmospheric absorption. Atmospheric conditions during the firings may be found in Table 1. It is assumed that the field of view was filled during the calibration and data scans. A conversion to the apparent radiant intensity of the plume can be accomplished by standard formulas, but that is fraught with difficulties; see Appendix A.

The calibration was accomplished using a globar collimated with an off-axis paraboloid of 50-in. focal length. The temperature of the globar was measured with an L&N optical pyrometer. The reflectivity of the mirror was assumed to be 0.94, and the emissivity of the globar was assumed to be unity. The radiance from the chopper blade is negligible compared with that of the globar or the missile plume. The spectral system calibration can thus be written as

$$K_\lambda = \frac{(N_\lambda)_G}{V_{det}} ,$$

where

K_λ is the spectral system calibration factor,

$(N_\lambda)_G$ is the calculated radiance of the globar,

and

V_{det} is the measured voltage at the detector. A sample globar curve is shown in Fig. 22, and the results of the calibration are shown in Fig. 23.

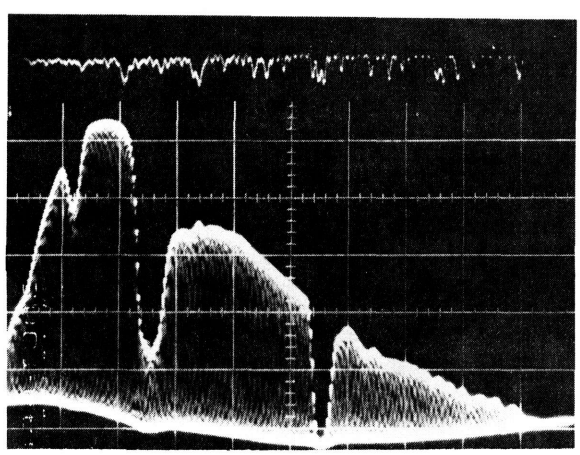

Fig. 22 - Globar calibration curve

Table 1
Meteorological Conditions

Date	Time	NOS Run No.	Wind		Air Temperature (°F)	Wet Bulb Temperature (°F)	Humidity (%)	cm/km Precipitable H_2O	Pressure, mm Hg	cm/198m Precipitable H_2O	Cloud Cover
			Velocity (knots)	Direction (deg)							
5-2-68	2305	1	2	280	58	53	72	0.86	759.0	0.17	Clear
5-3-68	0125	2	2	—	51	49	86	0.80	758.2	0.158	Clear
5-4-68	0121	3	0	—	68.25	63	75	1.29	753.8	0.255	Clear
	0255	4	4	160	60	58	78	1.06	754.8	0.209	Clear
	0427	5	0	—	—	—	—	—	754.8	—	Clear
	0531	6	—	—	56.5	56	96	1.11	754.8	0.219	80% Light rain
	0655	7	—	—	56	56	100	1.16	755	0.229	10%

The resolution of the system with 1-mm slit widths is shown in Fig. 24. The average resolution was about 0.06 μm. A summary of the system specifications is given in Table 2.

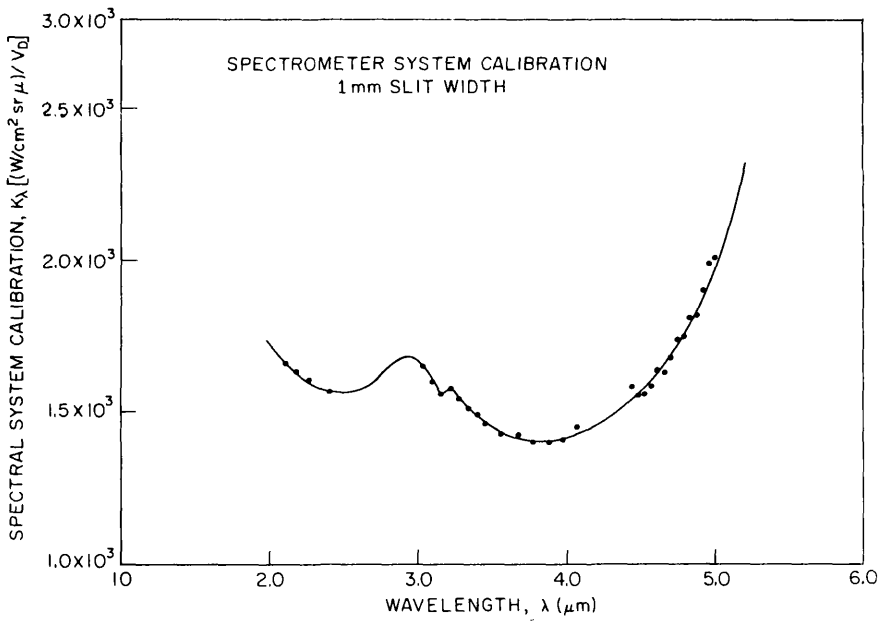

Fig. 23 - Spectrometer system calibration

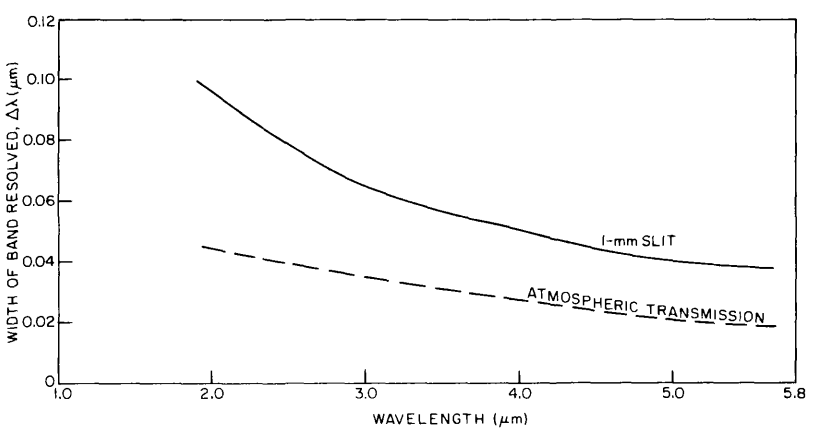

Fig. 24 - Resolution of spectrometer with 1-mm slits

Table 2
Spectrometer System Specifications

Scan Time:	0.1 sec
Instrument Type:	Prism Dispersion, LiF prism
Wavelength Range:	2.0 to 5.4 μm
Average Resolution:	0.06 μm (1-mm slits)
Field of View:	1.9 mrad x 9.3 mrad
Effective Aperture:	133 cm^2
f number, external optics:	$f/3.9$

SCANNING SPECTROMETER DATA REDUCTION

The raw data are in the form of photographs of a dual-beam scope trace, as in Fig. 25. A series of data points was selected along the spectrum signal for analysis (about 60 per spectrum). The points were chosen so that accurate interpolation was possible. For each point, the oscilloscope amplitude pattern was read in some unit converted to centimeters, and its projected position with respect to the wavelength marker pips determined. To convert to wavelength, the wavelength calibration curve was used. To convert the CRT amplitude to radiation units, the formula

$$N_\lambda = K_\lambda \left[\frac{S \cdot C}{G} \right]$$

was used, where

N_λ is the apparent spectral radiance of the target,

K_λ is the system calibration factor,

S is the scope gain settings in V/cm,

G is the amplifier gain setting,

and

C is the amplitude measurement in centimeters.

ACCURACY

Radiometer

The reproducibility with which the radiance responsivity R_N can be determined is about 5 percent. However, the absolute value of R_N may be in error by 25 percent.

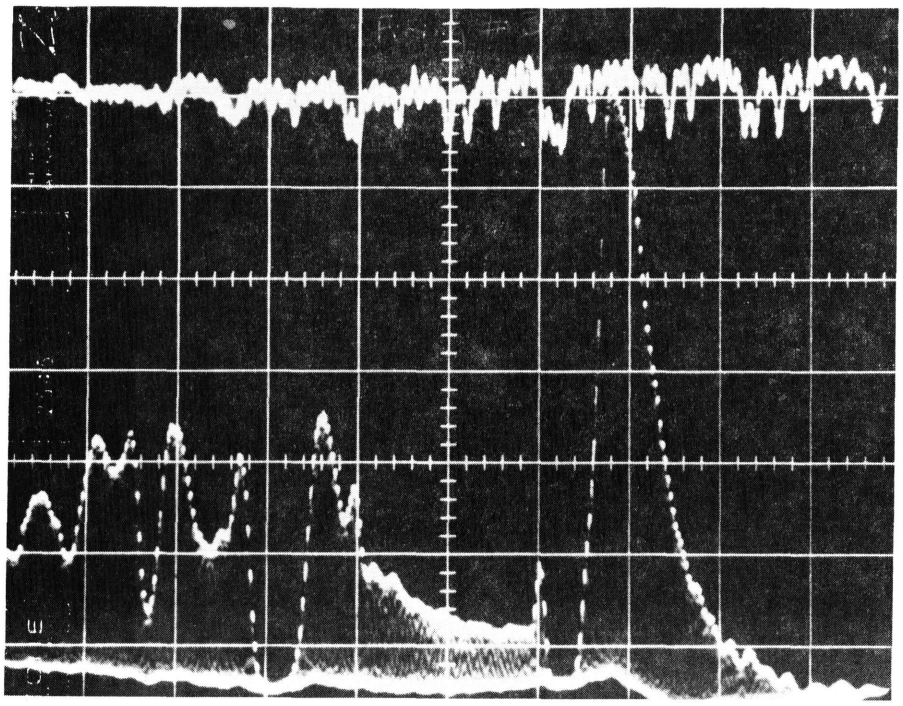

Fig. 25 - Photograph of spectrum from oscilloscope

Rapid Scanning Spectrometer

The accuracy of the wavelength calibration varies over the wavelength interval; it is 0.055 μm at 2 μm and 0.03 μm at 5 μm. The incident radiation is chopped at 4000 Hz, giving about 400 samples per spectra or about a 0.01-μm interval per sample. The error of the wavelength calibration curve is estimated to be less than 0.02 μm. The position of a point with respect to the wavelength marker is reproducible to 0.01 μm at 4.5 μm and to 0.025 μm at 2.0 μm. Thus, the overall wavelength error is less than $\pm$0.05 μm. As shown later in the discussion of the measurements, the wavelength calibration seems accurate to $\pm$0.02 μm.

The accuracy of the amplitude calibration is affected by several factors. The gain settings on the scope and amplifier are accurate to at least $\pm$5 percent. Noise from the detector, pickup in the leads, noise in the amplifier and scope, and washout in the film combine to give a "blurring" at the top and bottom of the amplitude excursion. These factors can be lumped into a "noise level," and determined by measuring the width of the CRT trace when the spectrometer aperture is closed. The level will vary with gain setting; with an average signal excursion of 2 cm on the crt, and a maximum measured CRT trace width of 0.2 cm, the noise introduces an uncertainty of about 10 percent. A negligible amount of uncertainty is introduced by ringing in the amplifier, which causes the varying baseline evident in Fig. 25. An estimated uncertainty of 20°C in the temperature

of the globar* used for calibrating the spectrometer introduced an uncertainty of about 9 percent in the radiance. Error in measuring the amplitude introduced an uncertainty of less than 5 percent. Thus, the total amplitude uncertainty is less than about 20 percent.

DISCUSSION OF RESULTS

Radiometric Data

There were seven firings of solid-propellant motors from Sidewinder and Chaparral missiles on May 2, 3, and 4, 1968. The firings were made at night to avoid picking up sunlight. The infrared radiation from the plumes was so much greater than the background radiation that the latter has been disregarded in the data reported here and in the formulas of Appendix A.

The run numbers listed in Table 3 are the consecutive numbers used by the Naval Ordnance Station and the corresponding numbers used by Block Engineering, Inc., to identify their data. Further information on the runs is listed in Ref. 3. This reference is primarily a table correlating the run numbers and information on later liquid-propellant motors, such as liner type, throat diameter, nominal oxidizer-to-fuel ratio, nominal chamber pressure, aspect angle, and comments on the firings. The latter items do not apply to the solid propellants.

On the first firing, both radiometers were overloaded by the large signals, and no absolute measurements were made. It will be seen in Table 3 that on runs 2, 3, and 4 the results are given in terms of radiance N whereas for runs 5, 6, and 7, the radiant intensity J is given. This is done because of the geometrical properties of the measuring instruments and the flame, which are discussed in detail in Appendix A. In the case of runs 2, 3, and 4, the field of view of radiometer B was entirely filled, hence accurate measurements of radiance in units of $W/cm^2 sr$ were possible. The effective field of view of this instrument is a square of 1.9 mrad on a side. Therefore, at 197 m the portion of the flame viewed would be a square of 37.6 cm on a side. Photographs taken of the firings were scaled, and the dimensions of the visible portion of the flame were determined. In the present case of a stationary rocket motor, the infrared radiating portion of the flame was found to be larger than the visible flame.

Since $J = NA$, where A is the area of the flame, it is necessary to know the radiating area to determine the radiant intensity from the radiance. Besides the fact that the area of the infrared portion of the flame is not known, its temperature is not uniform over the entire area. An estimate of the effective radiating area can be made by measuring the radiance with a small field-of-view and the radiant intensity with a large field-of-view instrument that encompasses the entire flame, and then solving for the area in the formula $J = NA$. This was done for the case of liquid-propellant motors where more data were available. These results will be given in a future NRL report. A rough estimate of the visual size when viewed from the side if 100 cm in diameter at the center and 250 to 350 cm long.

*This includes the calibration error in the pyrometer, variations along the length of the globar, and the change of globar temperature during calibration.

Table 3
The Radiance and Radiant Intensity of Solid-Propellant Motor Plumes

Date	Time	NOS Number	BEI Number	Wavelength Interval (μm)	Apparent Radiance, (W/cm^2 sr)	Apparent Intensity, J (W/sr)	Calculated Apparent Radiant Intensity, J (W/sr^1)	Aspect Angle	Instrument
5/2/68	2305	1	1A	–	–	–	–	90°	–
5/3/68	0125	2	1B	1.8-23	0.167	–	8350	90°	B
5/4/68	0120	3	2	4.38-5.19	8.1×10	–	2835	45°	B
5/4/68	0255	4	3	3.47-4.33	$0.262^*/3.06 \times 10^{-2\dagger}$	–	$9150^*/1071^\dagger$	45°	B
5/4/68	0427	5	4	1.45-4.4	–	$2547^*/1394^\dagger$	–	0°	A
5/4/68	0531	6	5A	3.95-4.7	–	1234	–	0°	A
5/4/68	0655	7	5B	3.32-4.3	–	$761^*/380^\dagger$	–	0°	A

*Peak value.
†Steady state value.

The field of view of the *A* radiometer was 11.1 mrad; therefore, at 198 m the projected area is 220 x 220 cm. This should certainly encompass the entire flame from a 0° aspect, hence on firings 5, 6, and 7, the results are given in terms of radiant intensity as measured by radiometer *A*. Notice that, in some cases, two values of radiance and radiant intensity are given; these refer to the peak value and what might be called a steady-state value. Figure 26 is a recording from NOS Run 5 showing these two values. It should be pointed out that the response of the recorder was about 1 second for full-scale deflection, so that the trace is slightly distorted. Note that the zero of the time shown does not coincide with the start of the firing.

A reasonable estimate for the effective radiating area of the plume in the infrared is about 50,000 cm^2 at an aspect angle of 90°. If the radiance values of column six in Table 3 are multiplied by this value for 90° aspect angles and by 35,000 cm^2 for the 45° aspect angles, the values of column eight in Table 3 are obtained.

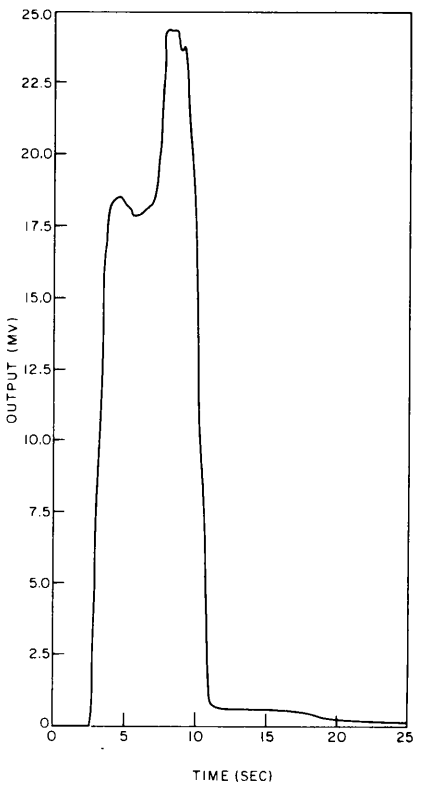

Fig. 26 - Radiometric recording of Run 5, filter 3A, full-scale deflection 26.18 x 10^{-3} W/cm^2 sr

Spectral Data

The reduced spectra for firings numbered 3 through 7 (or 2, 3, 4, 5A, and 5B, respectively, using the Block Engineering numbers) are presented in Figs. 27a through 27e. Firings 3 and 4 are at a 45° aspect, while 5, 6, and 7 are at ~3° aspect. (The latter firings were at a 0° aspect to instruments located ~30 feet to the side of the spectrometer.) The projected position and size of the field of view of the spectrometer with respect to the missile body and visible plume for the various firings are shown in Figs. 28a and b. Background scans were made at various times between firings and showed the radiation for the background to be far below the noise level of the system. One such scan is shown in Fig. 29.

The effects of atmospheric absorption are evident in the spectra. Indeed, the measured positions of the absorption valleys can be compared with published data for the valleys to give a check on the wavelength calibration. A low-resolution,* 1000-ft-path, atmospheric transmission curve (4) is shown in Fig. 30. An exhaustive tabulation was made of the absorption valleys shown in Fig. 30 and of those evident in each of the five spectra; the measured values differed from the published values by 0.02 μm or less. Fig. 30 can be compared with the spectra to demonstrate the correspondence in the positions of the absorption valleys. Absorptions not resolved are generally beyond the resolution band of the instrument, and are all quite weak.

*The resolution of the curve is shown in Fig. 24.

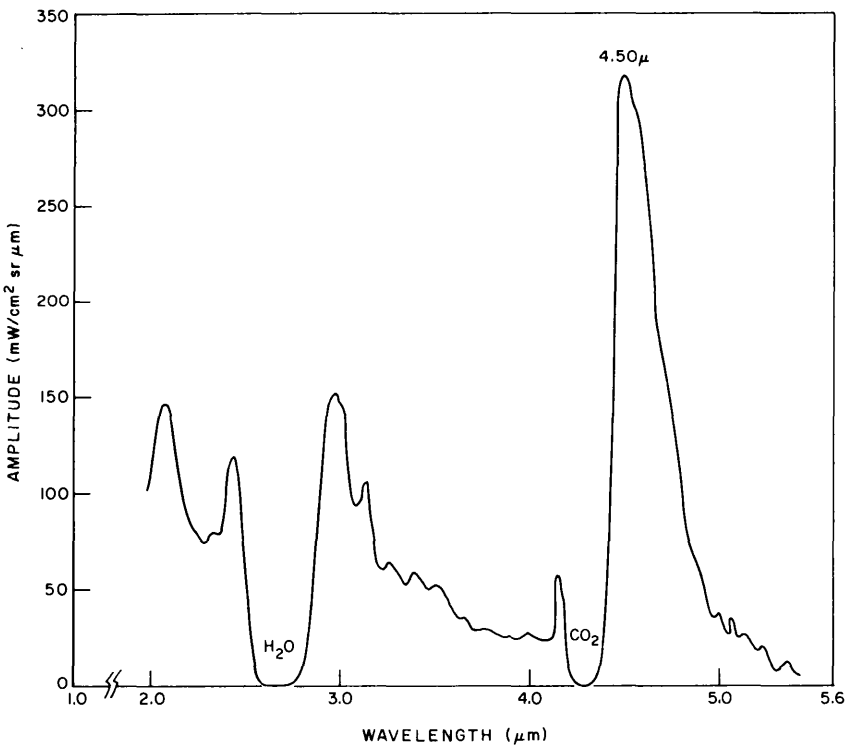

(a) NOS Run 3

Fig. 27 - Reduced spectrometer data

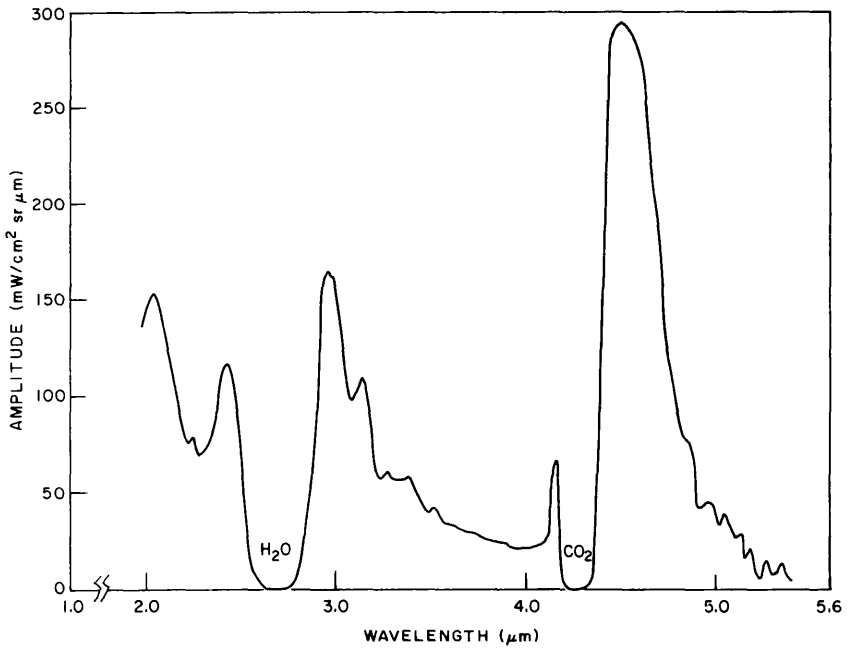

(b) NOS Run 4

Fig. 27 - Reduced spectrometer data (Continued)

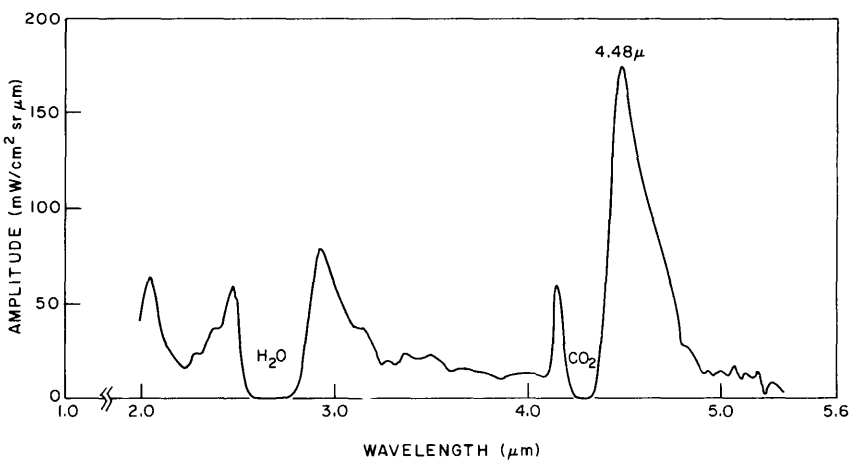

(c) NOS Run 5

Fig. 27 - Reduced spectrometer data (Continued)

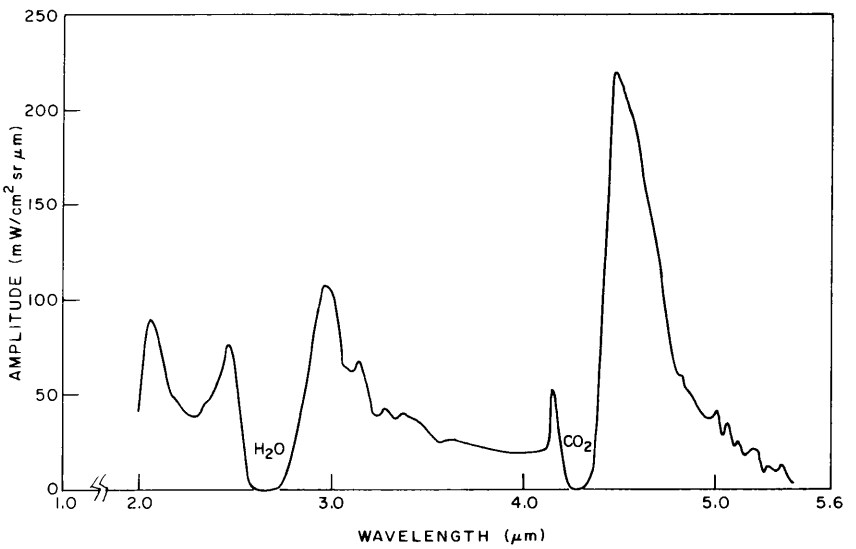

(d) NOS Run 6

Fig. 27 - Reduced spectrometer data (Continued)

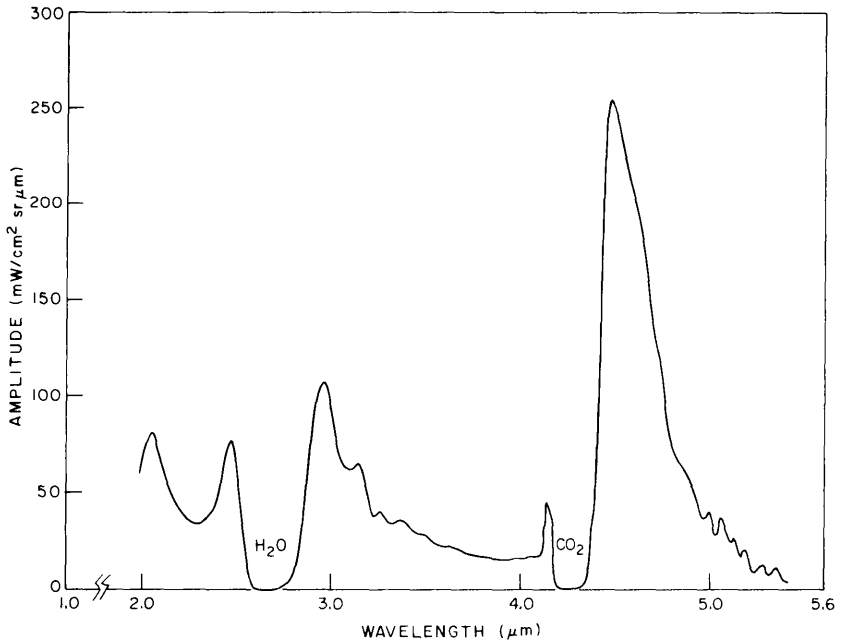

(e) NOS Run 7

Fig. 27 - Reduced spectrometer data (Continued)

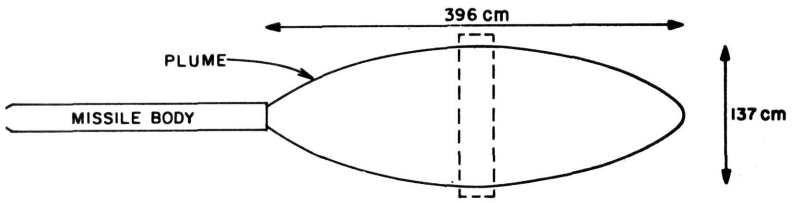

(a) Firings 3 and 4

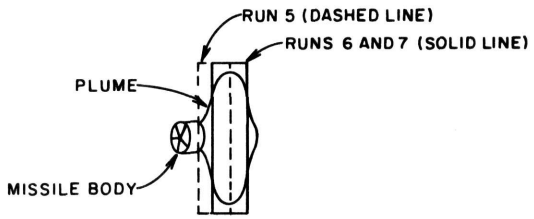

(b) Firings 7 through 9

Fig. 28 - Size of field of view projected on estimated IR plume

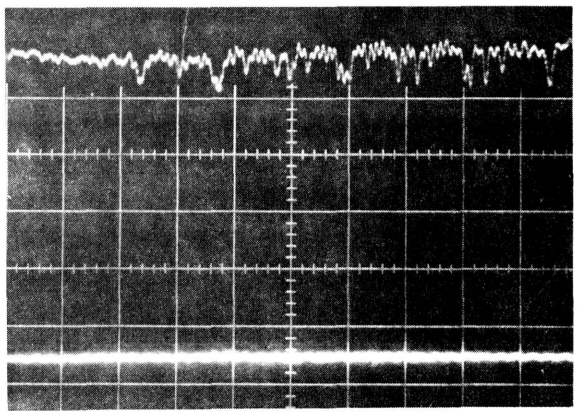

Fig. 29 - Spectrometer background noise

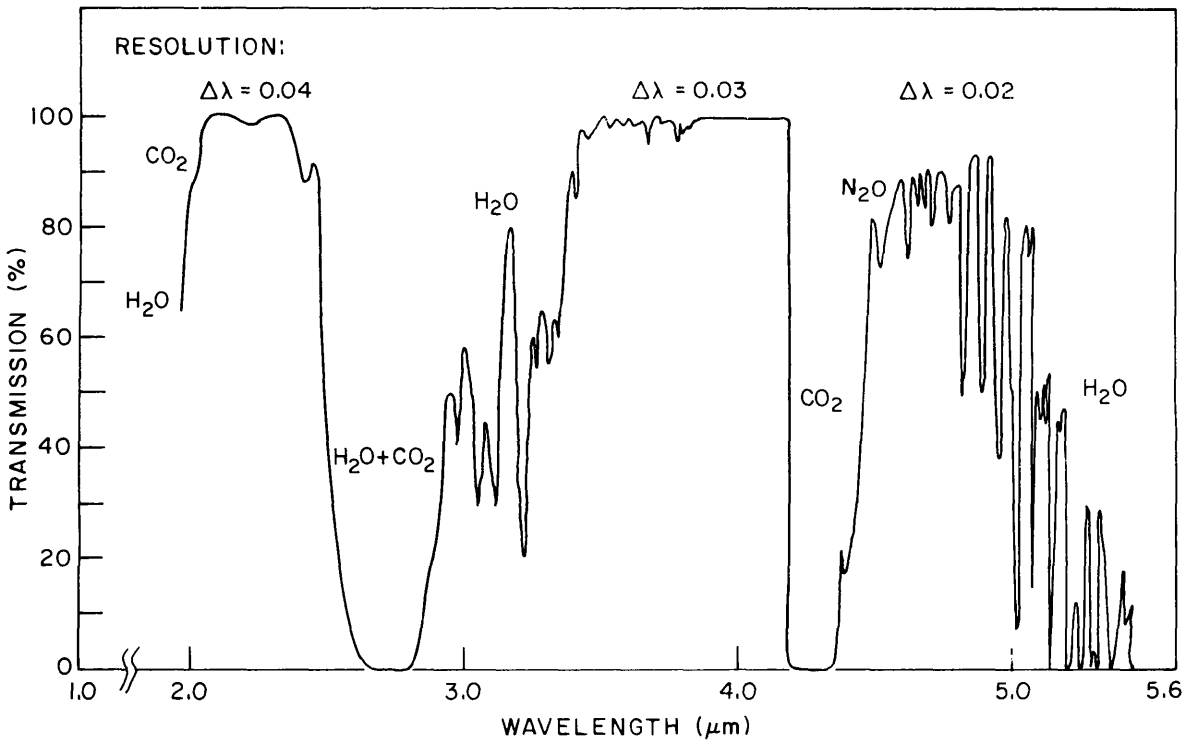

Fig. 30 - Low-resolution atmospheric transmission over a 1000-ft path, 2.0 to 5.4 μm (data from Ref. 4)

Certain emission peaks are also evident throughout the spectra. These peaks are listed in Table 4, with column three being simply the average of the observed peak values in mW/cm^2 sr μm and column four being the ratio of N_λ at a given wavelength to N_λ at 4.5 μm. Firing No. 5 has been excluded, as the relative position of the field of view (FOV) was not optimum for this run (cf. Fig. 28b). The peaks are grouped according to aspect, as there is evidence that there is somewhat less H_2O emission compared to CO_2 emission in the outer portions of the plume (predominant at the 3° aspect) than in the inner portions of the plume (effective at the 45° aspect). It should be noted that the two CO_2 peaks near 4.15 μm and 4.50 μm are from CO_2 emission due to the asymmetrical vibration ν_3, centered around 4.25 μm, with atmospheric absorption at 4.25 μm blocking the radiant energy in between these two "peaks" (5). There is perhaps a slight emission at about 4.7 μm, evidenced as a bulge in the wing of the CO_2 emission; this is attributed to CO emission (5).

To compare this data with the radiometric data taken simultaneously, a numerical integration from 3.47 to 4.33 μm was performed on Fig. 27b, which corresponds to the radiometer filter band for this firing. Table 3 shows that the radiometric measurement yielded 30.6 mW/cm^2 sr; the numerical integration gave 23 mW/cm^2 sr. Good agreement is evident.

Table 4
Emission of Gases

Origin*	45° Aspect			3° Aspect		
	Wave-length (μm)	Apparent Spectral Radiance, N_λ	Ratio of N_λ to N_λ at 4.5 μm	Wave-length (μm)	Apparent Spectral Radiance, N_λ	Ratio of N_λ to N_λ at 4.5 μm
CO_2	2.05	150	0.5	2.05	85	0.4
H_2O	2.43	118	0.4	2.47	77	0.3
CO_2, H_2O, OH	2.96	159	0.5	2.95	107	0.5
CO_2	4.15	67	0.2	4.15	49	0.2
CO_2	4.5	306	1.0	4.48	239	1.0
CO	4.75	—	—	4.7	—	—

*Ref. 5.

In this report, the radiance and radiant intensity values given are the effective values reaching the instruments and are not corrected for atmospheric attenuation. Point-by-point computations of the atmospheric transmission are not justified. Simpler methods which integrate the transmission over bands give misleading results, since the radiation is not backbody.

Table 1 lists some of the meteorological conditions existing during the tests. The wind was virtually still during the firings and, therefore, had little if any effect on the results. The air temperature, listed in column six of the table, varied from 51°F to 68.2°F. The relative humidity varied from 72 to 100 percent, and the precipitable water in the path between the firing site and the measurement site varied from 0.17 to 0.255 cm.

CONCLUSIONS

From the radiometric measurements, the apparent radiance of the flame at an aspect angle of 90° was found to be 0.167 W/cm^2 sr in the infrared region from 1.8 to 23 μm. If an area of 50,000 cm^2 and a uniform source are assumed, then the radiant intensity is 8350 W/sr. At a 0° aspect angle, the apparent radiant intensity was found to have a peak value of 1394 W/sr in the 1.45- to 4.4-μm region, 1234 W/sr in the 3.95- to 4.7-μm region, and 761 W/sr in the 3.32- to 4.3-μm region.

As expected, measurements of the flame made with a rapid-scanning spectrometer show that there was considerable atmospheric absorption over the relatively short path length of 198 m. The most pronounced absorption bands are those of H_2O and CO_2 at 2.7 μm and of CO_2 at 4.3 μm.

The sources of the emission peaks can be identified from the spectral measurements. These include CO_2 emission around 2.05, 2.96, 4.15 and 4.5 μm, H_2O emission around 2.43 and 2.96 μm, and evidence of CO emission at 4.75 μm.

The spectral data show that the spectral content of the solid rocket plumes is not significantly different from that of other kinds of hydrocarbon flames. The spectra of the flame was found to be very similar to that of a Bunsen flame burning natural gas; for example, see Ref. 5, Fig. IX (1). Spectra of flares and jet engines, if made under similar conditions, also are quite similar to those of the flames from the rocket motors.

ACKNOWLEDGMENTS

The authors acknowledge the able and considerable assistance of James Chapman, Tom Cindea, and Francis Steiger in preparing the instruments for the measurements and in gathering the data.

REFERENCES

1. Ellis, J.M., Matlack, D.E., Templin, H.A., and Black, G.M., "Airborne System for the Measurement of Infrared Missile Spectra," NOLTR 64-56, 1964

2. Downie, A.R., Magoon, M.C., Purcell, T., and Crawford, B., Jr., "The Calibration of Infrared Prism Spectrometers," J. Opt. Soc. Am. 43:941 (1953)

3. "Spectroscopic Measurement Program for Solid and Liquid Propellant Rocket Engines," DCL11/DNB 8010 Preliminary Report, Naval Ordnance Station, Indian Head, Md., June 1968

4. Yates, H.W., "The Absorption Spectrum from 0.5 to 25 Microns of a 1000-Ft Atmospheric Path at Sea Level," NRL Report 5033, Sept. 27, 1957, p. 5

5. Gaydon, A.G., "The Spectroscopy of Flames," New York:Wiley, pp. 166-170, 1957

Appendix A

CONSIDERATIONS IN THE REDUCTION OF RADIOMETRIC DATA

A radiometer can be used to measure either the radiance N (units W/sr cm^2) or radiant intensity J (units W/sr) of a target, depending upon the geometry of the physical arrangement of the target and radiometer and the manner in which the radiometer is calibrated. Of course, other quantities could be determined equally well, such as the irradiance H (units W/cm^2), at the radiometer. Three geometrical configurations were encountered in the measurements. In case I the field of view of the radiometer was completely filled by a portion of the target as shown in Fig. A1a; in case II the field of view was only partially filled by a portion of the target as in Fig. A1b; in case III the field of view of the radiometer was larger than the flame and viewed the entire target as in Fig. A1c.

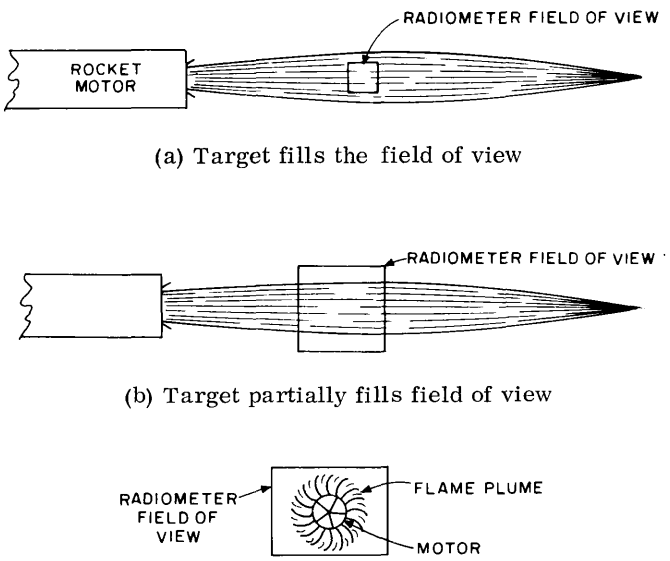

(a) Target fills the field of view

(b) Target partially fills field of view

(c) Target is smaller than field of view

Fig. A1 - Field of view projected on flame

In the following derivations, it is apparent that for case I the radiance N can be accurately measured, but to determine target's radiant intensity J its area must be known. For case II the area of the flame in the field of view must be known to determine either N or J. For case III, J can be measured directly, but the target area must be known to compute N.

Since the signals at the outputs of the radiometers (and spectrometer) were voltages, calibration constants are required to convert these voltages to radiometric quantities. For these tests two constants were determined experimentally. One constant, the irradiance responsivity R_H with units of $(V\ \mathrm{cm}^2)/\mathrm{W}$, was determined by calibrating the radiometers with a small source of known area and temperature. The second constant, the radiance responsivity R_N with units of $(V\ \mathrm{cm}^2\ \mathrm{sr})/\mathrm{W}$, was determined by calibrating the radiometers with an extended source that filled the fields of view.

The effective fields of view of the radiometers (especially instrument B with the immersed detectors) were about twice the calculated values based on the detector size and system focal length, because of imperfections in the optics. For this reason the ratio of R_N/R_H ($= \omega$, sr) was used in determining the effective solid angular fields of view of the instruments.

The radiance responsivity R_N is given by $R_N = V/N$, where V is the radiometer voltage corresponding to the radiance N. When an extended source is used for this calibration, N can be computed directly. Conversely, the radiometer can then be used to measure the radiance N of a target which fills the field of view as in case I. In this case $J = NA_T$, W/sr, where J is the radiant intensity of the target and A_T is target area. Therefore $J = (VA_T)/R_N$ but A_T may not be known so that $N = V/R_N$.

If the target partially fills the field of view of the radiometer as in Fig. A1b, the irradiance at the radiometer is

$$H = \frac{J}{D^2} = \frac{A_T N}{D^2} ,$$

where D is the distance from the target to the radiometer and A_T the area of the target seen by the radiometer.

The energy falling on the detector is $P = [(\pi d^2)/4]\, N\, (A_T'/D^2)$ W, where $(\pi d^2)/4$ is the effective mirror area A_M, and A_T'/D^2 is the solid angle subtended by the target. Hence,

$$P = A_M \frac{NA_T'}{D^2}, Watts$$

This energy produces a voltage

$$V = R_H \frac{NA_T'}{D^2}, Volts;$$

since $R_H = R_N/\omega$,

$$V = \frac{R_N}{\omega} N_T \frac{A_T'}{D^2}, Volts,$$

which is the equation for case II.

This is a more difficult case to evaluate than case I, since the exact value of A_T', the flame area seen by the radiometer, is not well defined.

Case III, in which the field of view of the radiometer is larger than the target area, is, like case I, a well-defined situation. To be precise the signal from the background should be included; however, the signals from the target were so much larger than background radiation that the latter was ignored.

As in case II, the voltage at the detector is

$$V = \frac{A_T N R_H}{D^2} ,$$

except that now A_T is the whole area of the target. Since $J = NA_T$,

$$V = \frac{JR_H}{D^2}$$

and

$$= \frac{JR_N}{D^2 \omega} ,$$

and the radiant intensity is measured directly as

$$J = \frac{VD^2 \omega}{R_N}$$

without further computations.

When the equations for cases I and II are applied to a target, the assumption is being made that the radiance from the target is the same over the entire target area.

DOCUMENT CONTROL DATA - R & D

(Security classification of abstract and indexing annotation must be entered when the overall report is classified)

1. ORIGINATING ACTIVITY *(Corporate author)* Naval Research Laboratory Washington, D.C. 20390	Group 3

3. REPORT TITLE

THE INFRARED RADIATION FROM SOLID-PROPELLANT ROCKET MOTORS
[Unclassified Title]

4. DESCRIPTIVE NOTES *(Type of report and inclusive dates)*
This is an interim report; work is continuing on the problem.

5. AUTHOR(S) *(First name, middle initial, last name)*

George L. Harvey and Jay D. Burch

6. REPORT DATE	7a. TOTAL NO. OF PAGES	7b. NO. OF REFS
May 29, 1969	40	5

8a. CONTRACT OR GRANT NO. NRL Problem R06-38 b. PROJECT NO. SF 23-372-006-9292 c. d.	9a. ORIGINATOR'S REPORT NUMBER(S) NRL Report 6899 9b. OTHER REPORT NO(S) *(Any other numbers that may be assigned this report)*

10. DISTRIBUTION STATEMENT
In addition to security requirements which apply to this document and must be met, each transmittal outside the Department of Defense must have prior approval of the Director, Naval Research Laboratory, Washington, D.C. 20390

11. SUPPLEMENTARY NOTES	12. SPONSORING MILITARY ACTIVITY Department of the Navy (Naval Ships Systems Command), Washington, D.C. 20360

13. ABSTRACT

The infrared radiation in the spectral region of 1.45 to 20 μm from stationary solid-propellant rocket motors of the Sidewinder type was measured using two radiometers and a rapid-scanning spectrometer. The measurements were made at a range of 200 m at aspect angles of approximately 90°, 45°, and 0° to the flame. The emission spectra were found to be similar to those of other kinds of hydrocarbon flames.

DD FORM 1 NOV 65 1473 (PAGE 1)

S/N 0101-807-6801

Security Classification

KEY WORDS	LINK A		LINK B		LINK C	
	ROLE	WT	ROLE	WT	ROLE	WT
Spectral emittance						
Solid-propellant motors, irradiation						
Infrared radiation						
Infrared detection						
Missile detection						
Plume detection						
Background discrimination						
Infrared spectroscopy						